Separation and Purification Technology 411 (2026) 139404

Contents lists available at ScienceDirect

Separation and Purification Technology

journal homepage: www.elsevier.com/locate/seppur

Evaluating the stability and efficiency of Fe(III)-DTPA complex for prednisolone degradation by solar photoelectro-Fenton process at neutral pH

Paola Tirira [a], Ivan Díaz-Redondo [a,b], Nuria López-Vinent [b], Minghua Zhou [c], Pere Lluís Cabot [a], Ignasi Sirés [a,*]

[a] Laboratori d'Electroquímica dels Materials i del Medi Ambient, Departament de Ciència de Materials i Química Física, Secció de Química Física, Facultat de Química, Universitat de Barcelona, Martí i Franquès 1-11, 08028 Barcelona, Spain

[b] Processos de Separació, Membranes i Polímers, Departament d'Enginyeria Química i Química Analítica, Secció d'Enginyeria Química, Facultat de Química, Universitat de Barcelona, Martí i Franquès 1-11, 08028 Barcelona, Spain

[c] Key Laboratory of Pollution Process and Environmental Criteria, Ministry of Education, College of Environmental Science and Engineering, Nankai University, 38 Tongyan Road, Tianjin 300350, China

ARTICLE INFO

Keywords:
Chelating agent
Fenton's reaction
Glucocorticoid
Hydrogen peroxide electrogeneration
Water treatment

ABSTRACT

The stability of the Fe(III)-DTPA complex for its use as a promising homogeneous catalyst to solve the pH bottleneck in solar photoelectro-Fenton (SPEF) process was evaluated for the first time. Viability depends on its resistance to photodegradation and attack by reactive oxygen species; ideally, it should allow sufficient release of free iron catalyst while preserving ligand stability to prevent iron precipitation. Here, Fe(III)-to-ligand molar ratio was first optimized to ensure complete chelation within a wide pH range, as well as high photostability against UVA and sunlight and resistance to $^{\bullet}OH$ attack. Results showed that Fe(III)-DTPA complex at ratios of 1:1 and 1:2 remained stable at pH 3–9 for at least 180 min. Notably, the 1:2 complex exhibited superior photostability and oxidative resistance during SPEF treatment, minimizing the iron precipitation. As a proof of concept, removal of the glucocorticoid prednisolone (PREDN) by SPEF at pH 7 was investigated. Complete degradation of 0.055 mM PREDN in 50 mM Na_2SO_4 medium containing 0.05 mM Fe(III)-DTPA (1:2) was achieved after 90 min at 30 mA cm^{-2}. Although 95% of the complex was also degraded, the organic species derived from iron complex maintained a significant percentage of soluble iron (> 40%). Additionally, phytotoxicity and QSAR tests revealed that an initially pronounced toxicity due to by-products generated from DTPA and PREDN resolved into a non-toxic mixture with enhanced biodegradability. Therefore, Fe(III)-DTPA complex (1:2) can be considered a sustainable catalyst for SPEF treatment of drugs at circumneutral pH, combining acceptable operational stability and environmental safety.

1. Introduction

Among the wide variety of pharmaceuticals detected in wastewater treatment plant (WWTP) effluents and freshwater systems, glucocorticoids (GCs) and antibiotics are ubiquitous [1]. These substances enter the water cycle pre-eminently through wastewater discharges from hospitals, pharmaceutical companies, and urban households [2–4]. In particular, GCs are commonly used to regulate essential physiological functions in vertebrates [5,6]. However, unintentional exposure can disrupt the normal functioning of humans and animals [2,7]. Of note, up to 20% of the administered GCs is not metabolized and hence, domestic, hospital and agro-industrial wastewater becomes potentially hazardous [8]. Prednisolone (PREDN), a synthetic glucocorticoid with anti-inflammatory properties [9], is one of the most frequently detected GCs in hospital wastewater (250 ng L^{-1}) [10] and industrial wastewater (2000 ng L^{-1}) [10]. Since the occurrence of COVID-19, higher concentrations, within the range of mg L^{-1}, have been reported [6]; this results from multiplied prescriptions of dexamethasone, prednisone and methylprednisolone to treat infected patients [10]. Notably, prednisone is essentially metabolized to PREDN [6,9], which explains the rising levels of the latter in aquatic environments; following the pandemic, studies reported PREDN concentrations reaching up to 0.448 mg L^{-1} in

* Corresponding author.
E-mail address: i.sires@ub.edu (I. Sirés).

https://doi.org/10.1016/j.seppur.2026.139404
Received 21 April 2026; Received in revised form 2 July 2026; Accepted 17 July 2026
Available online 17 July 2026

South African wastewater [6]. Conventional treatments are insufficient for effectively removing this type of pollutant, as demonstrated by the identification of PREDN residues in WWTP effluents (0.06 to 0.6 ng L^{-1}) [8], and receiving rivers (0.03 to 1083 ng L^{-1}) [8,11]. This phenomenon underscores the need for more advanced water treatment technologies [5].

In this context, advanced oxidation processes (AOPs), such as ozone, UV/H_2O_2, UVA/chlorination, and photo-Fenton have demonstrated effectiveness below 90% in removing GCs [2,5]. Among these methods, electrochemical AOPs (i.e., EAOPs) emerge as a promising alternative to remove persistent organic pollutants [10,12]. Despite their great potential for water decontamination, there is a limited number of studies specifically addressing the degradation of PREDN by EAOPs; in contrast, more attention has been paid to investigate the effect of operational parameters on antibiotics removal [3,13]. Recently, a study evaluated the removal of PREDN from water by homogeneous (dissolved ferrous iron as catalyst) and heterogeneous (rGO/Fe_3O_4/CF) electro-Fenton (EF) process; although both systems demonstrated a high PREDN removal, up to 84% and 75% after 120 min, respectively, their effectiveness was only tested under favorable acidic pH 4.5 [14]. EF process is the simplest Fenton-based EAOP, in which the crucial step is the in-situ H_2O_2 production upon cathodic reduction of injected O_2 (reaction (1)) [15]. In the presence of a catalyst that acts as a source of Fe(II), H_2O_2 is readily activated to hydroxyl radical ($^{\bullet}OH$), one of the most powerful oxidants (E^0 = 2.80 V vs. SHE), especially at optimal acidic conditions (pH ~ 3, reaction (2)) [16]. Nonetheless, the requirement of an acidic medium represents a significant limitation for the broad application of Fenton technology to the treatment of effluents at circumneutral pH, considering the additional time and cost for pH adjustment of large water volumes [15,17]. Likewise, EF process is limited by the slow regeneration of Fe(II) catalyst via reaction (3) (k_2 = 3.1×10^{-3} M^{-1} s^{-1}) [3,18]. To overcome this drawback, photo-assisted processes such as UVA and solar photoelectro-Fenton (PEF and SPEF, respectively) have been developed, demonstrating superior effectiveness for organics degradation. These two processes not only allow the generation of $^{\bullet}OH$ radicals via Fenton reaction [15], but also accelerate the Fe(II) photoregeneration (reaction (4)), further increasing the production of $^{\bullet}OH$ [19–21].

$$O_2 + 2H^+ + 2e^- \rightarrow H_2O_2 \quad (1)$$

$$Fe^{2+} + H_2O_2 \rightarrow Fe^{3+} + {}^{\bullet}OH + OH^- \quad (2)$$

$$Fe^{3+} + H_2O_2 \rightarrow Fe^{2+} + HO_2^{\bullet} + H^+ \quad (3)$$

$$[Fe(OH)]^{2+} + h\nu \rightarrow Fe^{2+} + {}^{\bullet}OH \quad (4)$$

The treatment of organic pollutants at neutral pH is certainly a major challenge for Fenton-based EAOPs. Recent advances have focused on the use of iron complexes as homogeneous catalysts, enabling Fenton and photo-Fenton reactions to operate at circumneutral pH [22–26]. Overall, these studies highlight the key role of the organic chelating agent, since the stability of the complexes against both oxidative degradation by $^{\bullet}OH$ and prolonged light exposure is a crucial requirement to ensure competitiveness against other AOPs; moderate to high stability of the chelator mitigates the iron precipitation and reduce fouling, which is essential because around 31% of the total treatment cost at large-scale is associated with fouling removal [27]. Several types of chelating agents have been investigated to treat organics and microorganisms at near-neutral pH by photo-Fenton process: ethylenediaminetetraacetic acid (EDTA), ethylenediamine-N,N′-disuccinic acid (EDDS), diethylenetriaminepentaacetic acid (DTPA), nitrilotriacetic acid, citric acid, and oxalic acid [21–35]. Despite the confirmed viability of these complexes in photo-Fenton, their application in Fenton-based EAOPs has been much less explored. For example, Fe(III)-EDDS complex was employed in PEF and SPEF treatments at neutral pH. Although the complex was proven very efficient for the removal of different organic pollutants, the poor stability of EDDS caused the gradual precipitation of iron [36–38]. This is detrimental because it would require an additional sludge removal unit, and periodical cleaning operations in the WWTP. A recent study evaluated the efficiency of humic acid (HA) as a chelating agent in EF for the removal of pharmaceuticals from actual urban wastewater; HA allowed keeping sufficient residual iron in solution, thereby enhancing the overall treatment performance [35].

In studies related to photo-Fenton process, organic chelators applied in fertilizers, such as DTPA, ethylenediamine-*N*,*N*′-bis(hydroxyphenylacetic acid) (EDDHA), and EDDS were comparatively employed for wastewater treatment at natural pH [25,37,39]. These studies demonstrated that DTPA and EDDHA have greater stability than EDDS. Although a slower degradation rate of the organic pollutants was observed, these chelates kept a high concentration of iron in solution throughout the treatment. In another study, DTPA, EDTA, and EDDS were employed to chelate Fe(II) for the photo-Fenton treatment of propranolol in agricultural wastewater at neutral pH using irradiation with LED lamps. The final pollutant concentration decay was analogous using either DTPA or EDDS (94% and 91% after 120 min, respectively); however, iron precipitation was significantly lower using DTPA (10% vs 97%) [31]. More recently, DTPA was applied to reinforce the performance of nano zero-valent iron (nZVI)/H_2O_2 in Fenton process for the abatement of sulfamethazine at circumneutral pH in simulated groundwater; DTPA was able to complex the Fe^{2+} ions released from nZVI, which minimized particle aggregation and the formation of passivating oxide layers [40].

Worth highlighting, DTPA is one of the most widely used chelating agents in industrial, agricultural, and domestic applications to avoid metal precipitation during the process [41,42]. DTPA is a non-toxic aminopolycarboxylate acid featuring five carboxylic groups and three nitrogen atoms (Fig. 1a), which collectively coordinate to metal ions [40], including Fe^{2+} o Fe^{3+}. Fe-DTPA complex shows a coordination number of seven, producing a pentagonal bipyramidal geometry (Fig. 1b) [43]. DTPA has been approved as a fertilizer by the European Commission [32], and is registered as a fertilizer product by the Spanish Ministry of Agriculture, Fisheries and Food [31]. Considering the high stability of Fe-DTPA complex in Fenton-like treatments [31,39,40], this chelating agent seems a promising alternative to EDDS for the treatment of organic pollutants by PEF and SPEF processes at neutral pH, although DTPA is more slightly persistent in both aquatic and soil environment [26,31]. Therefore, this research aims to: (i) Prepare Fe(III)-DTPA complexes at different Fe(III):ligand molar ratios, optimizing the chelation at various pH values; (ii) assess the photostability of each complex and its resistance to $^{\bullet}OH$ attack in PEF and SPEF treatments; (iii) evaluate the efficiency of Fe(III)-DTPA for the removal of PREDN from water at neutral pH by SPEF process; and (iv) measure the evolution of biodegradability and toxicity during selected trials.

2. Materials and methods

2.1. Chemicals

Sodium sulfate was provided by Merck; diethylenetriaminepentaacetic acid pentasodium salt solution (DTPA-Na_5), purum ~40% in H_2O ($C_{14}H_{18}N_3Na_5O_{10} \bullet xH_2O$), EDDS (as acid trisodium salt solution ~35% in H_2O), iron(III) perchlorate hydrate ($Fe(ClO_4)_3 \bullet xH_2O$), and prednisolone (PREDN, $C_{21}H_{28}O_5$) were obtained from Sigma-Aldrich; methanol of UHPLC supergradient quality, perchloric acid and ammonium acetate were acquired from Panreac; Fe(III)-DTPA (7 wt.% chelated iron) and Fe(III)-EDDHA (6 wt.% chelated iron) were purchased from Phygenera. *Tert*-butanol used as scavenger was supplied by Sigma-Aldrich. Reagent grade chemicals were employed for toxicity and biodegradability tests. Ultrapure water for all analyses was obtained from a Millipore Milli-Q system.

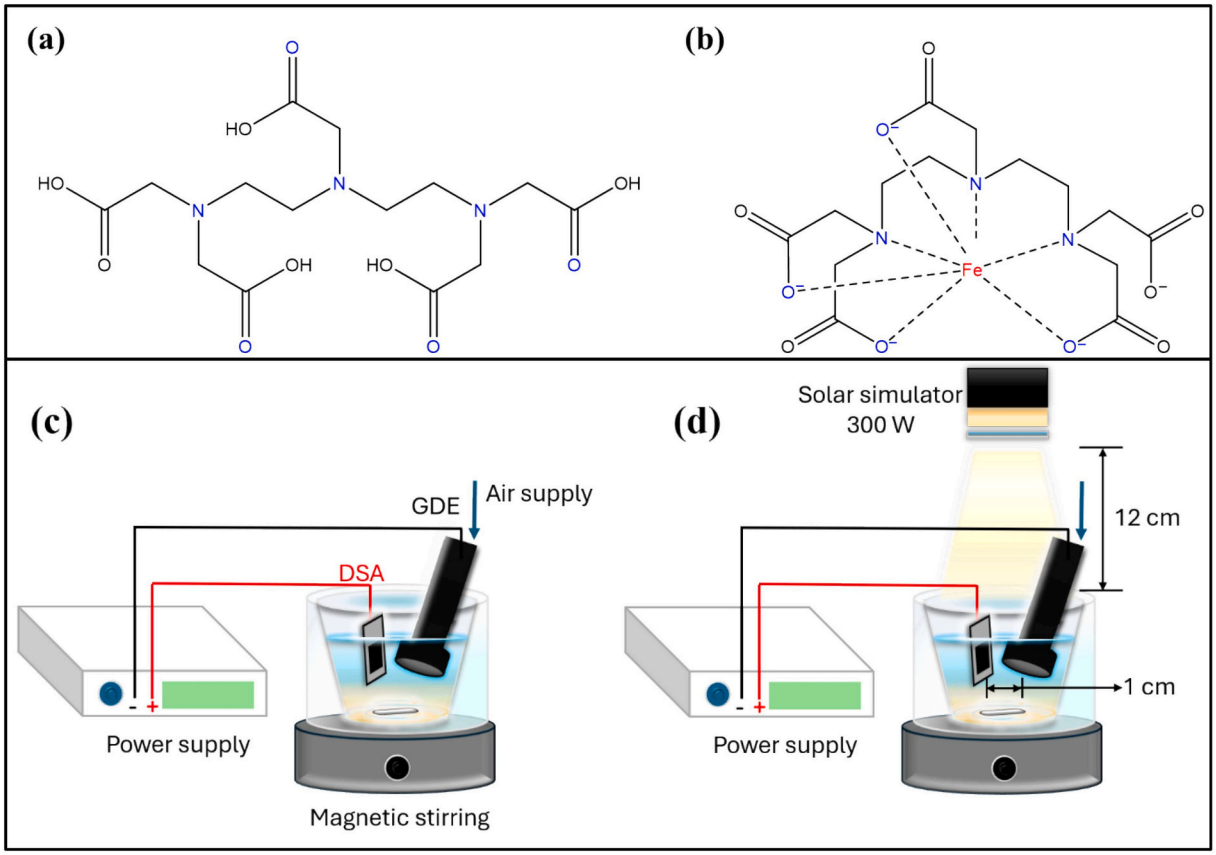

Fig. 1. Chemical structure of (a) DTPA and (b) Fe-DTPA complex. Scheme of the laboratory-scale batch reactor employed for (c) EF and (d) SPEF processes, operated under constant irradiation from a solar simulator equipped with a 300 W lamp. The electrochemical cell is equipped with DSA and GDE as the anode and cathode, respectively, both featuring an active geometric area of 3 cm^2.

2.2. Fe(III)-DTPA assays

2.2.1. Preparation of Fe(III)-DTPA complex

Fe(III)-DTPA complexes were synthesized at molar ratios 1:1 and 1:2. First, DTPA solutions were prepared at concentrations of 10 mM and 20 mM, at natural pH. Separately, a 10 mM $Fe(ClO_4)_3$ solution was made at pH 3. Subsequently, DTPA solution was gradually added dropwise into the iron solution under continuous magnetic stirring for 20 min, ensuring complete chelation. Fe(III)-DTPA 1:1 and 1:2 stock solutions containing 5 mM Fe(III) were stored in dark glass bottles at 4 °C. Under these storage conditions, the complexes remained stable for at least four days, as confirmed in Fig. S1.

2.2.2. Photolytic and electrochemical systems

All experiments were performed in an undivided, jacketed glass cell (100 mL volume) thermostatically maintained at 25 °C and stirred at 700 rpm. For the electrochemical trials, a DSA® anode (Ti|RuO_2, 3 cm^2 exposed area) and a gas-diffusion electrode (GDE, 3 cm^2 geometric area) were employed. These electrodes are commercial and were selected because of their availability and robustness in industrial electrochemical process. Air was directly supplied to the GDE chamber at a flow rate of 400 mL min^{-1} to promote the electrochemical generation of H_2O_2. The electrodes were placed in the center of the cell and separated by 1 cm from each other (Fig. 1c). Constant current was applied using an Amel 2051 potentiostat-galvanostat, and potential was monitored with a Demestres 605 Digital multimeter. Solar photolysis and SPEF experiments were carried out using an LS300Xe solar simulator equipped with a 300 W high-pressure Xenon lamp (LOT-QuantumDesign), with emission wavelength range of 250–2500 nm (Fig. 1d); solutions treated by UVA photolysis and PEF trials were irradiated with a UV black light blue tube lamp (Philips TL/6 W/08), emitting at a maximum wavelength of 360 nm. Both lamps were placed at 12 cm above the solution surface. The cell was covered in all tests with aluminum foil to prevent photon loss.

All tests were made in 100 mL of 50 mM Na_2SO_4 solution, at an initial pH 7. The Fe(III)-DTPA stock solution (5 mM Fe(III)) was directly diluted in the reactor to achieve the required initial concentration for each test.

2.3. Prednisolone degradation

The degradation of PREDN was carried out in 100 mL of 50 mM Na_2SO_4 solutions containing 0.055 mM PREDN –corresponding to total organic carbon (TOC) of 13.98 mg L^{-1}–, and 0.05 mM Fe(III)-DTPA (1:2) complex. These degradation tests were performed in the previously described reactor. Comparison tests using other complexes were performed by adding 0.05 mM Fe.

Most experiments were performed in duplicate, and when the obtained values were not fully consistent, a third replicate was carried out.

2.4. Analytical methods

According to previous studies, the absorption peak of the complex is proportional to the chelate concentration [28]. Consequently, the maximum absorbance wavelength of Fe(III)-DTPA complex was determined using a UV/Vis Specord 210 PLUS spectrometer (INYCOM) over the range of 240 nm to 450 nm at intervals of 1 nm. Fe(III)-DTPA and PREDN concentrations were analyzed by ultra-fast liquid chromatography (UFLC, Shimadzu Prominence LC-20 A) equipped with a Spherisorb® ODS2 Waters C18 column (150 mm × 4.6 mm, 5 μm), whose

outlet was connected to a photodiode array detector (SPD-M10A) set at 245 nm for PREDN and 260 nm for Fe(III)-DTPA complex. The autosampler and column were maintained at 4 °C and 35 °C, respectively. Isocratic elution was carried out with a mobile phase consisting of 20 mM ammonium acetate and methanol (40:60, *v/v*) at a flow rate of 0.25 mL min^{-1}, with an injection volume of 20 μL. TOC was determined on a Shimadzu VCSN analyzer using the non-purgeable organic carbon (NPOC) method, with an injection volume of 50 μL, and removal of the inorganic carbon by acidifying with concentrated H_2SO_4.

H_2O_2 concentration was assessed using the titanium colorimetric method; the absorbance was measured at 408 nm on a Shimadzu 1800 UV/Vis spectrophotometer. Iron content was quantified globally as total soluble iron using the 1,10-phenanthroline method (ISO 6332) in a Unicam UV/VIS spectrophotometer at 510 nm. All samples were filtered using 0.22 μm Clarify filters to remove precipitated iron. Dissolved O_2 was not monitored, since the H_2O_2 electrogeneration process was controlled by the air flow rate fed to the GDE rather than by the comparatively low amount of the dissolved gas.

2.5. Toxicity and biodegradability tests

The toxicity was evaluated in terms of phytotoxicity using *Lactuca sativa* (lettuce) seeds, purchased from a commercial supplier, following the methodology described by Zucconi et al. [44,45] and standardized protocols [46,47]. The tests were conducted in 100 mL of 12.5 mM Na_2SO_4 solution, since its conductivity (2.6 mS cm^{-1}) is similar to that typically determined for urban wastewater; the solution also contained 0.055 mM PREDN and 0.05 mM Fe(III)-DTPA (1:2), at an initial pH 7. Control assays were carried out using the same electrolyte solutions, along with added catalase solution to stop the degradation reaction and preserve the samples prior to analysis. Results were expressed as germination index (GI) percentages, calculated according to equations described in Text S1. Biodegradability was assessed by measuring the biochemical oxygen demand (BOD) of the initial solution (0 min) and sample collected after 90 min of treatment. These determinations were conducted following the 5210-D Biochemical Oxygen Demand (BOD) procedure from Standard Methods [48]. The methodology for *in-silico* quantitative structure-activity relationships (QSAR) analysis is described in detail in Text S2.

3. Results and discussion

3.1. Effect of pH on the Fe(III)-DTPA complex behavior

The occurrence of complete chelation of Fe(III) at a concentration of 0.1 mM with DTPA, at 1:1 and 1:2 molar ratios, was evaluated within a pH range of 3.0 to 9.0 and monitored over time. At both ratios, the Fe (III)-DTPA complex exhibited a maximum absorption wavelength at 270 nm regardless of the pH value (Fig. S2). In contrast, free DTPA absorbed only below 230 nm (Fig. S3), demonstrating that excess DTPA could not interfere with the absorbance monitoring for the complex. Likewise, as shown in Fig. S4, no variation in absorbance was observed over the wide pH range, demonstrating that the complexes remained stable under acidic, neutral, and alkaline medium for at least 180 min, which is an important feature for selecting the iron chelating agent [27]. This behavior is consistent with the pH-dependent speciation of the Fe (III)-DTPA system reported by Liu et al. [49], in which the protonation state of the coordinated DTPA changes across the studied pH range (more details in Text S3). Speciation calculations indicate that Fe(III) remains predominantly complexed with DTPA. At pH 7, the $[Fe(III)\text{-}DTPA]^{2-}$ species accounts for approximately 97.5% (Eqs. (S9) and (S10)), confirming that the complex is the dominant form under the experimental conditions. Moreover, the high overall stability constant of the Fe(III)-DTPA complex strongly favors the complex formation under all conditions investigated. Assuming a 1:1 Fe(III):DTPA stoichiometry, the calculated free Fe^{3+} concentration under the experimental conditions (0.1 mM Fe(III), 0.2 mM DTPA, pH 7) is 2.51×10^{-29} M (Eq. (S11)), indicating that the amount of free iron is negligible, and precipitation is not expected. In this context, previous studies have emphasized that a minimum molar ratio of 1:1 (iron-to-ligand) is necessary for effective iron chelation. In some cases, a higher ligand ratio can improve the complete iron chelation [23,30,31]. In this study, complete iron chelation was achieved at both 1:1 and 1:2 ratios at a wide pH range; when the molar ratio was increased to 1:2, no substantial enhancement in complex formation was observed. Nevertheless, it is important to note that higher ligand ratios may mitigate destabilizing factors such as the attack of $^{\bullet}OH$ and photons over the complex. For this reason, the effect of molar ratio under oxidation and photodegradation conditions was subsequently studied, highlighting its potential role in optimizing chelation efficiency.

3.2. Effect of Fe(III):DTPA molar ratio under exposure to UVA light, sunlight and $^{\bullet}OH$

The Fe(III)-DTPA molar ratio must be optimized to improve the operation conditions for water treatment by EF, PEF, and SPEF processes. Despite its importance, there is currently no available information regarding the influence of this factor on the performance of EAOPs. Worth noting, a suitable chelating agent for Fenton-like processes is required to fulfill two key criteria: (i) Absorb UV–Vis radiation to facilitate the photochemical reactions, and (ii) maintain a high concentration of soluble iron at neutral pH to ensure high catalytic efficiency [25]. Therefore, this work investigated the photostability of Fe (III)-DTPA complexes at 1:1 and 1:2 molar ratios in 100 mL of 0.050 mM Na_2SO_4 solution containing 0.1 mM chelated Fe(III) at pH 7.0. As shown in Fig. 2a-b, at both ratios, degradation was almost negligible (< 5%) for 90 min under dark and natural light conditions. In contrast, under UVA light irradiation, Fe(III)-DTPA (1:1) was slightly degraded (about 14%), whereas at a 1:2 ratio the concentration remained stable. Instead, simulated sunlight generated more pronounced effects: 42% of the 1:1 complex was degraded, while that at 1:2 ratio only underwent 12% degradation. These differences can be justified by the spectral properties of the complex, since Fe(III)-DTPA absorbs primarily around 260 nm, extending up to 450 nm. Consequently, simulated sunlight, which covers a broad wavelength range including this absorption bands, is more effective at promoting degradation, whereas the narrower UVA range (315–400 nm) overlaps less significantly with the absorption spectrum of the complex, resulting in lower photodegradation. The enhanced photostability at higher ligand ratios can be attributed to free DTPA molecules recapturing iron ions released during photodegradation of bound ligands, thereby reducing iron precipitation [23]. In addition, Fig. 2c demonstrates the minimal production of iron sludge, since at both ratios, less than 5% of iron precipitation was observed in all processes. Although both Fe(III)-DTPA complexes showed slightly higher degradation percentages under solar photolysis; the total iron concentration in solution remained unchanged. This can be explained by the photodissociation of Fe(III)-DTPA promoted by ligand-to-metal charge transfer excitation (LMCT) under UVA or solar irradiation, followed by the photoreduction of Fe^{3+} to Fe^{2+} (Eq. (4)), which remains soluble at neutral pH [30,37,50]. Consequently, the total iron concentration at the end of the processes remained constant. For comparative purposes, the photostability of Fe(III)-EDDS complex (0.1 mM, 1:1 molar ratio) was also evaluated (Fig. S5). Under solar irradiation, Fe(III)-EDDS (1:1) complex was completely degraded within 60 min, and 95% by UVA exposure after 90 min. Moreover, this complex presented poor stability even under natural light exposure, since its degradation started after just 60 min. These results are in full agreement with previous reports, which suggested that 80% of Fe(III)-EDDS was degraded after 5 h of simulated sunlight irradiation (15 W lamp) [51]. Another study investigated the degradation of sulfamethoxazole by simulated solar photolysis and reported that EDDS was significantly less stable than DTPA, resulting in 70% of iron precipitation with EDDS and only 8% with DTPA [39].

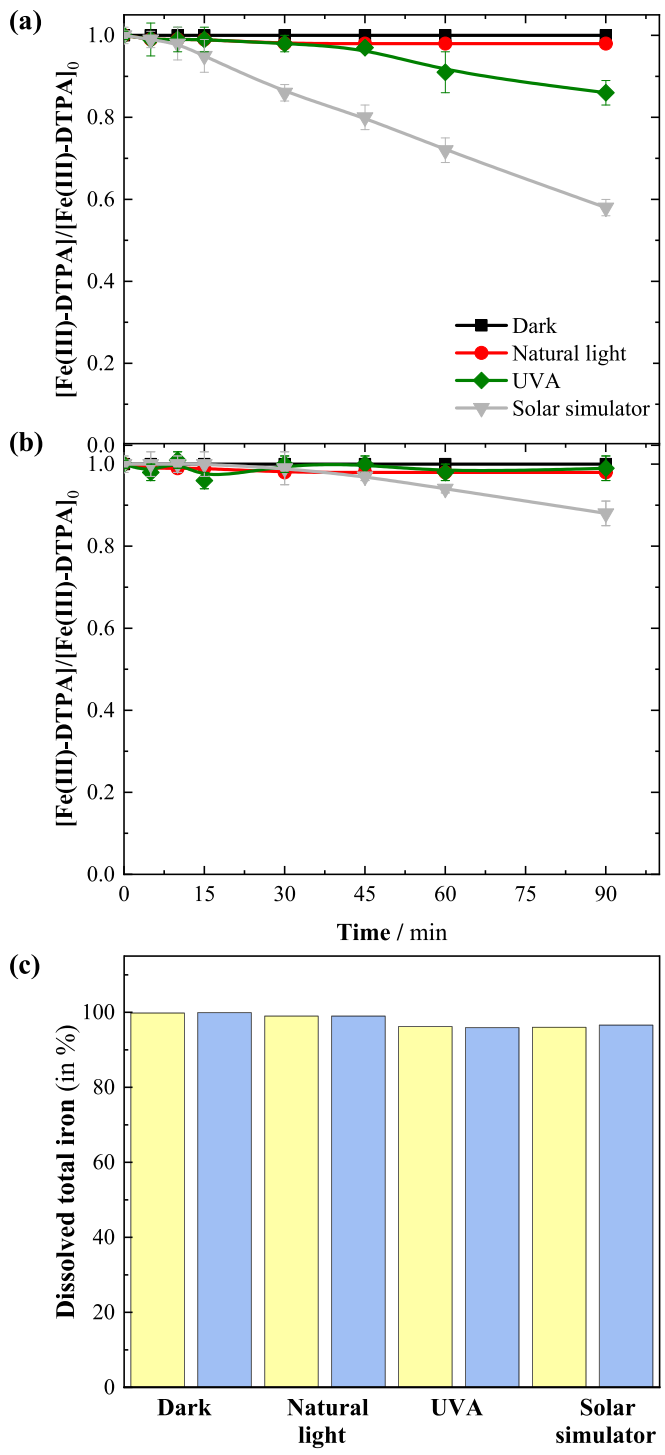

Fig. 2. Photostability of Fe(III)-DTPA complex at different molar ratios under various irradiation conditions. Normalized concentration decay of Fe(III)-DTPA complex at (a) 1:1 and (b) 1:2 molar ratio. (c) Comparison of the percentage of dissolved total iron at 90 min employing different molar ratios (yellow: 1:1; blue: 1:2). The experiments were performed in 100 mL of 0.050 M Na_2SO_4 solutions containing 0.1 mM Fe(III) at pH 7 and 25 °C. (For interpretation of the references to colour in this figure legend, the reader is referred to the web version of this article.)

Therefore, the clear superiority of DTPA represents a significant advantage for PEF and SPEF processes at neutral pH because it reduces the degradation of the complex to photoproducts and keeps a higher concentration of dissolved iron catalyst.

Likewise, the influence of •OH attack on the behavior of Fe(III)-DTPA complexes at 1:1 and 1:2 M ratios was investigated using the same electrolytic solution with 0.1 mM of chelated iron, applying a current density of 10 mA cm^{-2}. PEF and SPEF tests were performed using a UVA lamp and the simulated sunlight, respectively. In Fig. 3, it is shown that the 1:1 complex undergoes faster degradation as compared to the 1:2 complex across all EF, PEF, and SPEF processes. The greater stability of the latter is particularly evident in SPEF; the 1:1 complex was completely degraded after 90 min, while the 1:2 complex showed only 60% degradation at that time. These results demonstrate that the higher availability of free DTPA ensures that iron ions released in solution from photodegradation or oxidation of Fe(III)-DTPA can be recaptured. As a result, a favorable condition emerges for accelerating the Fenton's reaction, thereby increasing the •OH production and minimizing the iron precipitation [23,52]. The reaction mechanism of Fe(III)-DTPA has not been previously defined; however reactions (5)–(9) have been adapted

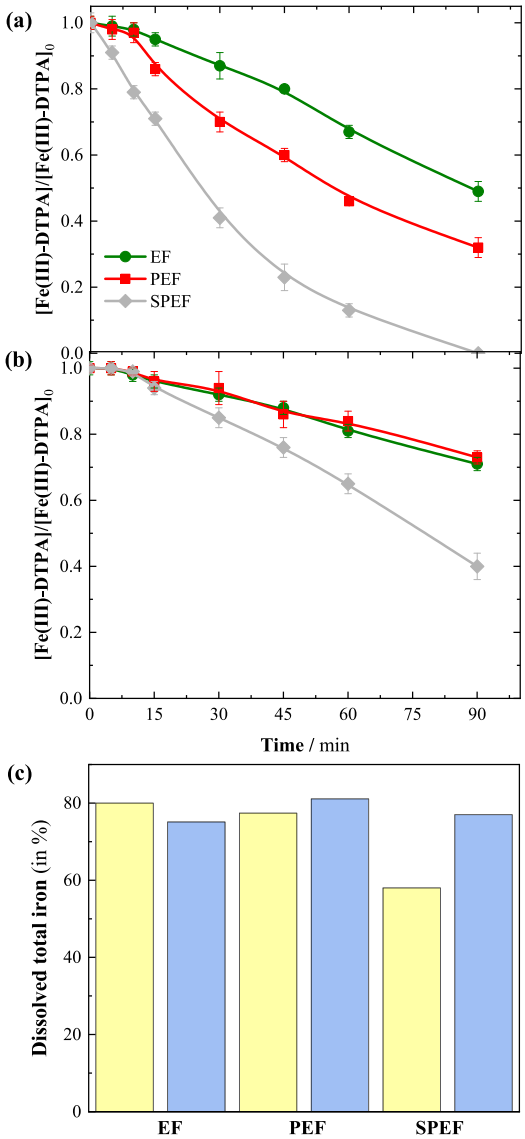

Fig. 3. Normalized concentration decay of Fe(III)-DTPA complex at (a) 1:1 and (b) 1:2 molar ratio under electro-Fenton (EF), photoelectro-Fenton with UVA light (PEF) and solar photoelectro-Fenton (SPEF) conditions. The trials were made in 100 mL of 0.050 M Na_2SO_4 solutions containing 0.1 mM Fe(III) at pH 7 and 25 °C, using a DSA/GDE cell at 10 mA cm^{-2}. (c) Comparison of the percentage of dissolved total iron at 90 min employing different molar ratios (yellow: 1:1; blue: 1:2). (For interpretation of the references to colour in this figure legend, the reader is referred to the web version of this article.)

based on mechanisms established for other chelating agents [25,34,53]. This mechanism allows understanding the fundamental steps and intermediates involved in the photodegradation or oxidation of this complex. The evolution of precipitated iron was determined as well (Fig. 3c). Fe(III)-DTPA (1:2) consistently led to the lower amount of precipitated iron; under SPEF conditions, only 20% of iron was precipitated after 90 min, while the use of 1:1 complex increased the iron precipitation, reaching 40%. The iron mass balance was carried out to evaluate the distribution of iron species after treatment, as well as to determine the percentage of precipitated iron (Table S1). In addition, a comparative test was performed to verify the contribution of DTPA ligand to the degradation of PREDN by the SPEF process at 30 mA cm^{-2}. Our results clearly highlight its key role. In the absence of DTPA, PREDN degradation after 90 min was approximately 30% lower (Fig. S6a). Moreover, a large fraction of iron precipitated (~82%, Fig. S6b), drastically reducing the amount of soluble iron and promoting sludge formation. These findings confirm that DTPA is essential to maintain iron in solution and to enhance the overall efficiency of the SPEF process. Likewise, to determine the contribution of anodic oxidation on the DTPA degradation, a separate experiment was carried out in the presence of 0.1 mM DTPA at the highest current density, and the possible ligand instability was monitored by TOC analysis. After 90 min, the TOC decreased slightly from 16.0 to 15.3 mg L^{-1}, indicating a limited but measurable effect of anodic oxidation on DTPA (Fig. S7). Based on these results, Fe(III)-DTPA complex at 1:2 molar ratio is revealed as highly promising for its application in EF-based water treatment processes. Its remarkable photostability and resistance to oxidative degradation ensure that iron can remain in solution even under stress conditions ($h\nu$, $^{\bullet}OH$). These findings support that Fe(III)-DTPA (1:2) can be potentially hypothesized as a reliable and robust catalyst for SPEF treatments.

$$\text{Fe(III)-DTPA} + h\nu \rightarrow [\text{Fe(III)-DTPA}]^* \rightarrow \text{Fe(II)-DTPA} \quad (5)$$

$$\text{Fe(II)-DTPA} + H_2O_2 \rightarrow \text{Fe(III)-DTPA} + {}^{\bullet}OH + OH^- \quad (6)$$

$$\text{Fe(II)} + H_2O_2 \rightarrow \text{Fe(III)} + {}^{\bullet}OH + OH^- \quad (7)$$

$$\text{Fe(III)-DTPA} + {}^{\bullet}OH \rightarrow \text{Fe(III)-DTPA}_{ox} \quad (8)$$

$$[\text{Fe(III)-DTPA}_{ox}]^* \rightarrow \text{Fe(II)} + \text{DTPA}^* \quad (9)$$

3.3. Prednisolone removal efficiency using Fe(III)-DTPA (1:2) complex

3.3.1. Effect of current density

The efficiency of Fe(III)-DTPA complex at 1:2 molar ratio as a homogenous catalyst in SPEF process was evaluated by employing a solution of 100 mL 0.050 M Na_2SO_4 with 0.055 mM PREDN at initial pH 7, carrying out several trials at different applied current values. The 1:2 ratio was selected based on its superiority stability, as discussed above. In order to avoid increasing the TOC content too much in the system, a low concentration of Fe(III)-DTPA 1:2 complex (0.050 mM, ~2.80 mg L^{-1} Fe(III)) was employed. As depicted in Fig. 4a, PREDN concentration decayed by nearly 80% after 90 min at 10 mA cm^{-2}. When the current was doubled to 20 mA cm^{-2}, PREDN degradation was not improved. However, complete removal of the pollutant was achieved at 30 mA cm^{-2} under analogous conditions; the complex also underwent 95% degradation (Fig. 4b). It is worth noting that, although the Fe(III)-DTPA complex was almost completely degraded, 1.18 mg L^{-1} of iron (~43% of the initial concentration) still remained in solution (Fig. 4c). This outcome can be attributed to the ability of the oxidized chelating products to keep iron in solution, as well as the presence of some free DTPA molecule able to recapture the free iron ions released during the reaction described in reaction (7).

Concurrently, the electrogeneration of H_2O_2 was studied; the highest H_2O_2 accumulation was achieved at 30 mA cm^{-2}, as expected from the fastest O_2 reduction (Fig. S8a). The current efficiency (CE) was

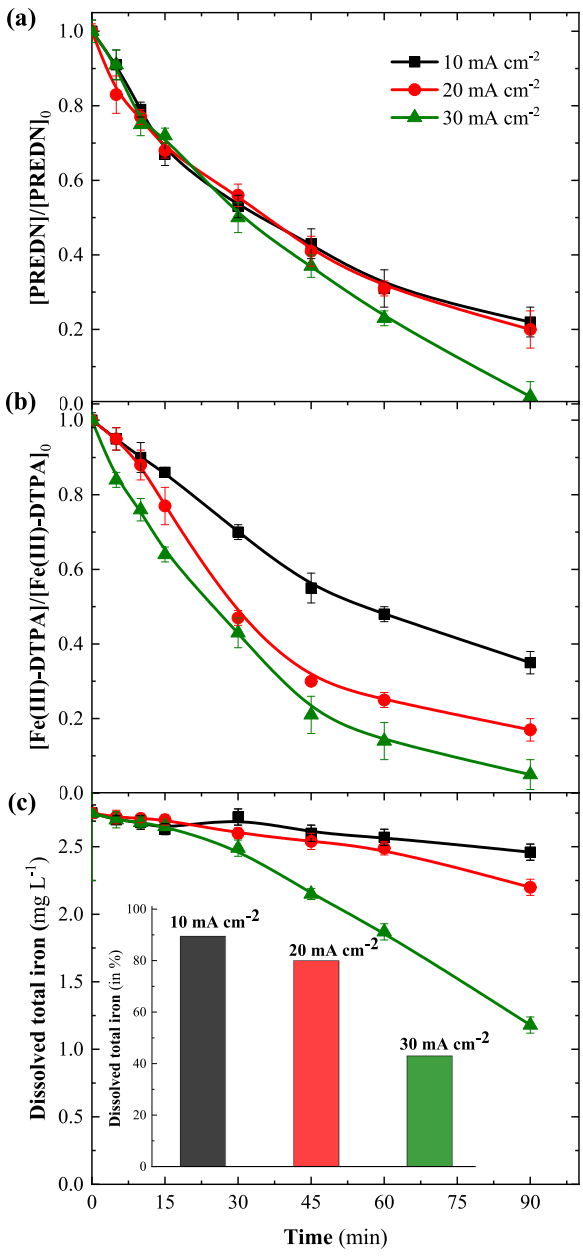

Fig. 4. Changes in normalized concentration of: (a) PREDN, (b) Fe(III)-DTPA complex, and (c) concentration of dissolved total iron over time during SPEF treatment at different current densities. The percentage of dissolved total iron remaining at 90 min is shown in the inset. The trials were carried out in 100 mL of 0.055 mM PREDN +0.050 M Na_2SO_4 solutions containing 0.050 mM Fe(III)-DTPA (1:2) at pH 7 and 25 °C.

calculated using the Eq. (S12) given in Text S4. The highest current efficiencies (≥80%) were achieved during the first minute, but their values decreased to about 60% at 30 mA cm^{-2} (Fig. S9). This behavior is expected in an undivided cell, where parasitic reactions and anodic H_2O_2 consumption occur in the same compartment. In addition, energy consumption (EC) was evaluated using Eq. (S13), obtaining increasing values at higher current densities (Fig. S10). Although the highest applied current resulted in a higher energy consumption and lower current efficiency, it was selected because it enables the effective degradation of the PREDN. Nevertheless, for future scale-up, the operation current density should be optimized. In contrast, when 0.05 mM Fe(III)-DTPA was added under simulated sunlight (Fig. S8b), the accumulation of H_2O_2 significantly decreased due to its rapidly

decomposition via Fenton's reaction. These findings confirm the efficiency and stability of the Fe(III)-DTPA (1:2) complex as a catalyst in SPEF processes. The complex enables an efficient pollutant degradation while maintaining enough iron in solution at neutral pH.

3.3.2. *Comparison of PREDN degradation by other processes*

The degradation of PREDN by other processes such as electro-oxidation (EO), UVA and solar photolysis, EF and PEF, was compared with that achieved in SPEF. All experiments were conducted in a 0.050 M Na_2SO_4 solution containing 0.055 mM PREDN at pH 7. For Fenton-based processes, 0.050 mM of Fe(III)-DTPA was added at 1:2 molar ratio, and the electrolytic treatments were conducted at 30 mA cm^{-2}.

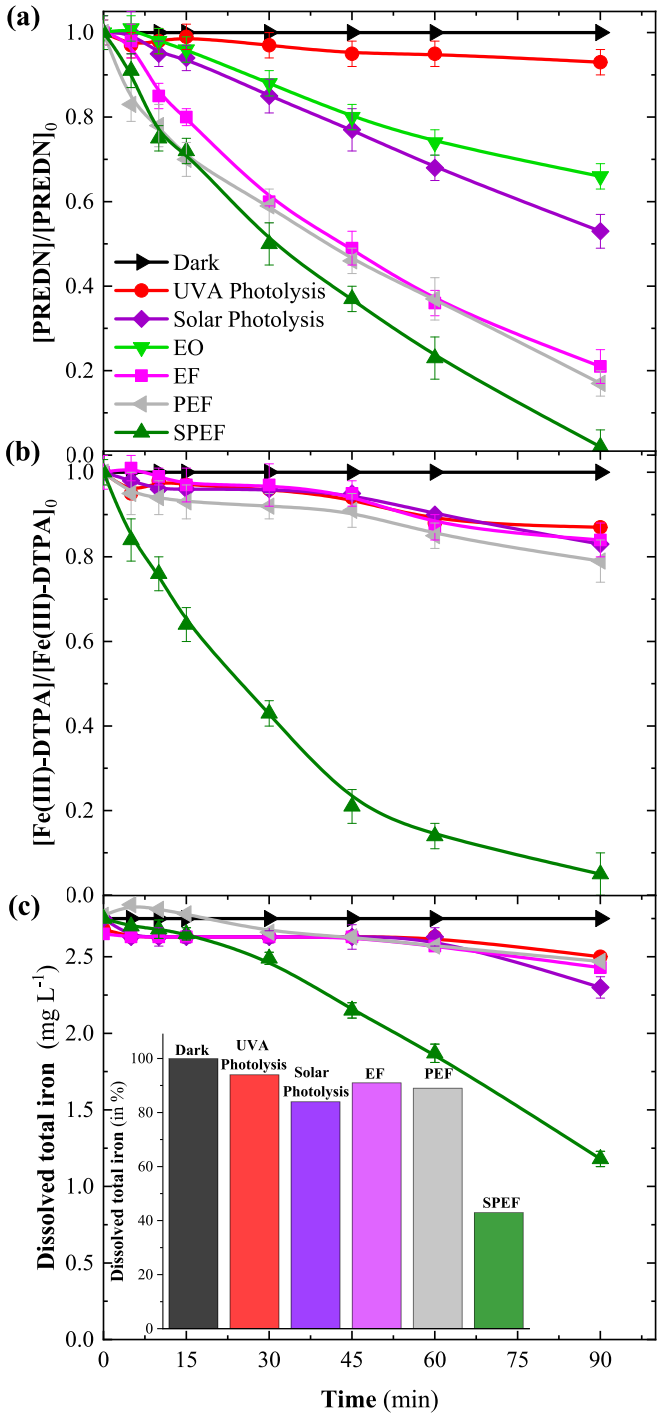

Fig. 5. Analogous to Fig. 4, comparing the performance of different treatments. The electrochemical tests were made at 30 mA cm^{-2}.

Fig. 5a shows that PREDN remained stable in the dark, whereas it was more susceptible to degradation under solar irradiation than UVA light, achieving 47% and 7% concentration decay, respectively. This behavior is not unexpected, as PREDN exhibits a pronounced absorption peak at approximately 245 nm, within the UV region covered by the solar spectrum (which starts over 200 nm). In contrast, the UVA source (315–400 nm) shows little overlap with the absorption spectrum of the pollutant, since PREDN displays negligible absorbance beyond 300 nm. Therefore, direct photolysis is reasonably larger under sunlight radiation. In the absence of the iron catalyst (EO process), 34% of PREDN was degraded. In contrast, EF, PEF, and SPEF processes demonstrated significantly higher efficiencies; EF and PEF achieved 79% and 83% removal, respectively. The similar performance of EF and PEF can be attributed to the limited irradiance of the UVA lamp to the system, which is insufficient to promote a larger photoreduction of Fe(III) to Fe (II) via photo-Fenton reaction. This limitation hampers the Fe(III)/Fe(II) redox cycle, eventually reducing the generation of $^{\bullet}OH$ radicals. Consequently, the inability to increase the $^{\bullet}OH$ production led to similar pollutant removal rates in both processes. Fig. 5b depicts the abatement of the Fe(III)-DTPA (1:2) complex, which exhibited high stability under UVA irradiation and sunlight, with only minor degradation in most treatments except under SPEF conditions, where disappearance reached 95%. To further elucidate the main reactive oxidant species, *tert*-butanol (*t*-BuOH) was employed as $^{\bullet}OH$ scavenger. A concentration 10 times higher than the maximum accumulated H_2O_2 concentration was used to ensure an effective excess of scavenger relative to the oxidant generated during the process. Under these conditions, PREDN removal decreased to only 22% after 90 min, confirming the predominant role of $^{\bullet}OH$ in the SPEF process (Fig. S11). Therefore, the higher degradation of Fe(III)-DTPA under SPEF can be attributed to several synergistic effects: direct photolysis, enhanced $^{\bullet}OH$ radical generation due to the efficient photoreduction of Fe(III) to Fe(II), and additional $^{\bullet}OH$ formation from the photolytic cleavage of H_2O_2, which absorbs strongly in the 200–300 nm range, overlapping with solar radiation.

In contrast, the difference in PREDN degradation between PEF and SPEF is moderate. Although SPEF can generate a larger amount of $^{\bullet}OH$ radicals via both Fe(III) photoreduction and H_2O_2 photolysis, the effect on PREDN is limited because iron precipitation under solar irradiation reduces the sustained production of radicals. Additionally, a significant fraction of $^{\bullet}OH$ reacts with H_2O_2 and DTPA itself, whereas PREDN is less competitive for radical attack due to its lower second-order rate constant with $^{\bullet}OH$ (1.1×10^9 M^{-1} s^{-1}) [9] as compared to DTPA (2.3×10^9 M^{-1} s^{-1}) [54]. Although PREDN might undergo some direct photolysis, this is partially masked by photon competition with H_2O_2. Together, these factors explain why SPEF strongly enhances Fe(III)-DTPA degradation, whereas the improvement in PREDN removal compared to PEF is modest. Fig. 5c shows the evolution of total dissolved iron over time. Fe (III)-DTPA (1:2) complex was highly effective in maintaining iron in solutions during all treatments, except in SPEF process, where a noticeable decline was observed. In most processes, the concentration of dissolved Fe remained nearly constant for 90 min; these results reaffirm the stability of the Fe(III)-DTPA (1:2) complex against both photo-degradation and oxidation by $^{\bullet}OH$. It should be highlighted that, even during the SPEF treatment, although 95% of complex was degraded, 43% of iron was kept in solution at neutral pH. These findings highlight the robust stability of Fe(III)-DTPA (1:2) catalyst and its oxidized species under AOPs, specifically in Fenton-based processes at circumneutral pH, which are typically limited to acidic range and often result in significant sludge formation after post-neutralization processes. In addition, the persistence of 43% iron in solution demonstrates that oxidized DTPA byproducts retain a residual chelating capacity, implying that only a minor fraction exists in a free state or mineralized. This residual chelating ability may benefit agricultural reuse by maintaining essential micronutrients in solution for plant uptake, potentially reducing fertilizer requirements in irrigation systems.

3.3.3. PREDN removal with other Fe(III) complexes

For comparative purposes, PREDN degradation by SPEF process was also carried out using Fe(III)-EDDS, at 1:1 molar ratio, which was chosen according to reported studies in which this proportion was previously optimized [38,55], and commercial Fe(III)-DTPA fertilizer. As illustrated in Fig. 6a, the use of these two compounds led to a faster PREDN removal as compared to the analogous trial with Fe(III)-DTPA (1:2) complex; specifically, the complete degradation was achieved within 45 min. In particular, Fe(III)-EDDS allowed accelerating the pollutant removal rate during the first 15 min, outperforming the commercial Fe(III)-DTPA fertilizer. However, its performance declined thereafter, likely due to the poor complex stability, which initially provides readily available dissolved iron ions but quickly leads to subsequent iron precipitation that decelerates the degradation kinetics [27]. This trend can be corroborated in Fig. 6b, where 90% of Fe(III)-EDDS was degraded at the end of the treatment. Fe-DTPA fertilizer presented a similar PREDN removal profile to Fe(III)-EDDS but, as aimed, the fertilizer showed a lower degradation percentage (69%). These differences in stability were further reflected in the percentage of dissolved iron remaining in solution (Fig. 6c). Fe(III)-EDDS (1:1) was the least stable, retaining only 33% of iron in solution, whereas Fe(III)-DTPA fertilizer maintained nearly 70%, demonstrating also a high resistance to both •OH attack and solar photons. In contrast, PREDN degradation using Fe(III)-DTPA (1:2) complex was slower, requiring 90 min for the complete removal; in turn, the use of this complex produced the lowest percentage of precipitated iron, with only 24%. Although Fe(III)-EDDS allows a faster degradation rate compared to Fe-DTPA fertilizer and synthetic Fe(III)-DTPA (1:2), its use as catalyst in Fenton-based processes is accompanied by a significant percentage of precipitated Fe. On a large scale, a low stability of chelated iron becomes a major operational challenge because it may be necessary to add higher concentrations of chelated Fe to counterbalance the accelerated precipitation, as well as the installation of additional sludge removal units following the treatment. Likewise, at present, EDDS is not commercially available in sufficiently large volumes for industrial applications, which would result in very high costs for full-scale installation [27]. Conversely, Fe(III)-DTPA sacrifices some kinetic efficiency with a well-balanced preservation of dissolved iron. Its excellent stability allows the application of lower Fe(III)-DTPA dosages, which minimizes the iron discharge into the effluent and can even facilitate the reuse of treated water. This trade-off highlights the operational and environmental advantages of Fe(III)-DTPA when envisaging upscaling, since it eliminates the need for pH adjustment and reduces both the sludge production and the presence of dissolved iron in the effluent. Another crucial remark arises from the fact that Fe(III)-DTPA is widely used as iron fertilizer in agriculture, ensuring its commercial availability in large volumes. To further evaluate the potential applicability of other commercially available iron fertilizers, a degradation test was also performed with Fe(III)-EDDHA. The results indicated that PREDN removal reached 70% after 90 min and dissolved total iron measurements showed that 60% of iron remained in solution (Fig. 6). This finding suggests that Fe(III)-EDDHA may represent another potential catalyst for SPEF treatment, which could be optimized to improve its efficiency.

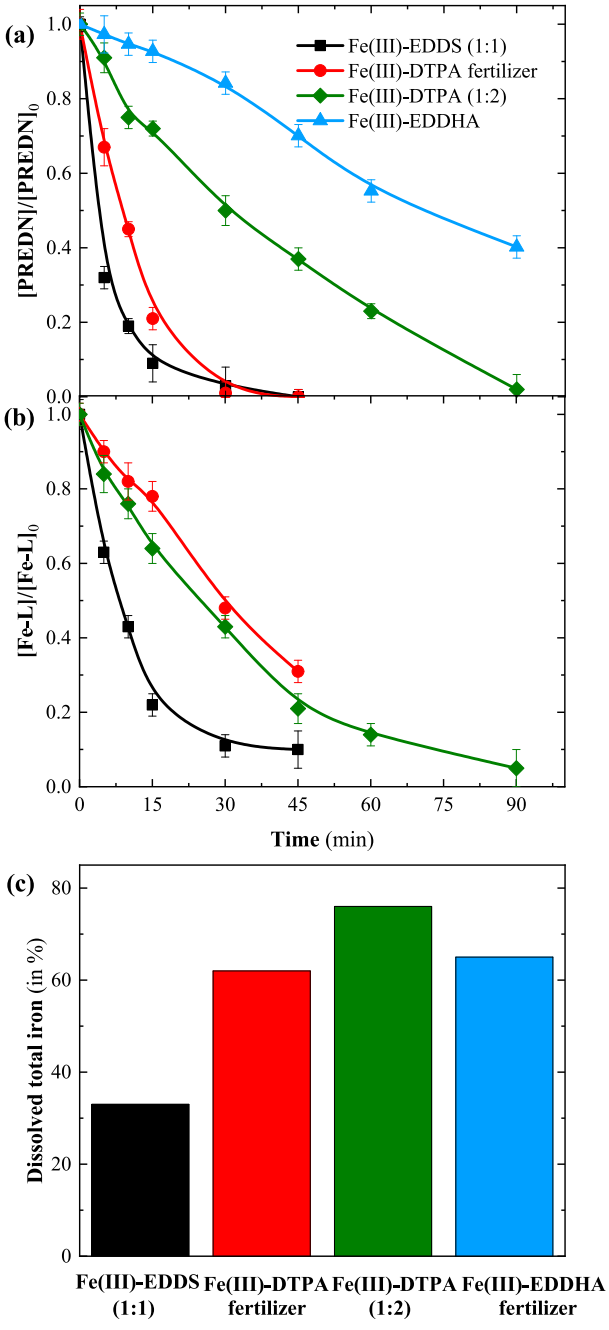

Fig. 6. Changes in normalized concentration of: (a) PREDN, (b) Fe-L complex, and (c) concentration of dissolved total iron over time during SPEF treatment, using different chelating agents (L) containing 0.050 mM Fe. The percentage of dissolved total iron remaining at 90 min is shown in the inset. The operation conditions were those described in Fig. 4, at 30 mA cm^{-2}.

To better contextualize these findings, Table S2 summarizes representative photo-Fenton and EF systems operating at circumneutral pH. The comparison highlights the frequent applications of EDDS, which often achieves complete degradation of target pharmaceuticals under mild pH conditions. A significant drawback, however, is that EDDS is typically consumed during the process. While alternative chelating agents and heterogeneous catalysts have been investigated, they frequently fail to attain full degradation. Consequently, our results support the potential of Fe(III)-DTPA as an effective alternative for circumneutral Fenton-based treatments.

To further evaluate the performance of SPEF treatment under more realistic conditions, PREDN removal experiments were carried out in actual wastewater effluent from a municipal treatment plant. The wastewater characterization is summarized in Table S3. To work with this complex matrix, the current density was reduced to only 10 mA cm^{-2} and the treatment time extended to 120 min to manage competing species. Despite the matrix complexity, over 61% degradation was achieved (Fig. S12). This performance is acceptable considering that dissolved organic matter and inorganic anions including carbonates (HCO_3^-/CO_3^{2-}), chloride (Cl^-), and sulfate (SO_4^{2-}) (Table S3), which act as •OH radical scavengers [35], Therefore, SPEF process catalyzed by Fe(III)-DTPA (1:2) remained robust and effective, validating its potential for actual wastewater remediation.

3.4. Biodegradability and toxicity analysis

The removal of PREDN from aquatic environments is relevant because some studies demonstrated that this drug can change the sexual characteristics of male and female fishes [56,57], even at low concentrations [8]. Additionally, the toxicity toward plants has not been studied in detail so far. Since this work proposes the use of an iron complex typically employed in agriculture, treated PREDN effluents could be potentially reused for irrigation; hence, it is reasonable to evaluate the impact of treated PREDN solutions on plant growth. Here, phytotoxicity tests were carried out by assessing the effect on *Lactuca sativa* germination and root development, and the results were expressed as GI (percentage values). Fig. 7 demonstrates no toxic effects from both PREDN/Fe(III)-DTPA (1:2) and Fe(III)-DTPA (1:2) control systems. The GI values consistently exceeded 100% throughout the experimental timeline for both conditions. In the presence of PREDN, GI decreases between the first 5 and 15 min, suggesting the formation of more toxic by-products during the early stages of PREDN degradation. This drop is remarkably corroborated by the absolute multi-trophic QSAR profiling (Fig. 8). Early structural variants like prednisone (TP-358) exert negligible toxicity alterations, remaining within the parent baseline values (LC_{50} of 82.61 mg L^{-1} for *Daphnia magna* and 5.09 mg L^{-1} for Fathead minnow). However, a distinct, transient toxicity peak occurs with mid-stage intermediates. Vertebrate toxicity crosses the "highly toxic" boundary threshold at TP-300 (LC_{50} = 0.52 mg L^{-1}) and TP-274 (LC_{50} = 0.71 mg L^{-1}). Concurrently, maximum invertebrate hazard shifts into the "moderately toxic" classification region for TP-288 (LC_{50} = 4.99 mg L^{-1}) and TP-286 (LC_{50} = 7.37 mg L^{-1}). This hazard behavior is strongly tied to a spike in lipophilicity, as the bioconcentration factor (BCF) increases from a baseline of 6.49 to peak limits of 80.53 (TP-288) and 84.29 (TP-286). This increased lipophilicity facilitates passive transport across biological membranes, enhancing cell bioaccumulation and explaining the short-term phytotoxicity observed in the seed assays [58]. Subsequently, the GI values increased progressively with time, reaching a maximum of 194% at 60 min and following a slight decrease to 171% at 90 min. These results indicate that neither Fe(III)-DTPA (1:2) complex and its degradation products, nor intermediates formed during PREDN degradation exhibited phytotoxic effects on seed germination. This late-stage detoxification is validated by the low molecular-weight aliphatic fragments (TP-116 and TP-74) and terminal dicarboxylic species like oxalic acid (TP-90), which safely shift into the "practically non-toxic" regulatory regime (LC_{50} values significantly exceeding 100 mg L^{-1}, peaking at 3667.85 mg L^{-1} for TP-116) accompanied by a drop in bioaccumulation potential (BCF ≤ 2.20). This final safety milestone is further confirmed by the terminal components of the DTPA pathway, including iminodiacetate (TP-133), ethylenediaminemonoacetic acid (TP-118) and glycine (TP-75), all of which populate the "practically non-toxic" regulatory domain and exhibit completely negligible bioaccumulation limits.

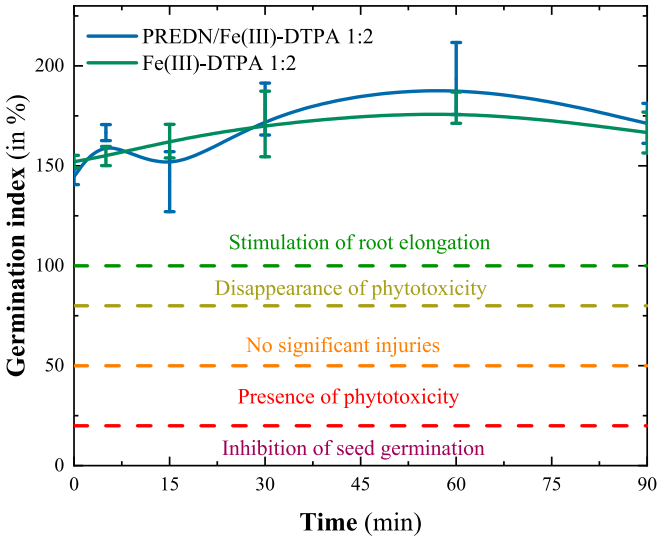

Fig. 7. Percentage of germination index of L. *sativa* exposed to samples collected at different times during the degradation of PREDN by SPEF process. The trials were carried out in 100 mL of 0.0125 M Na_2SO_4 solutions, with or without 0.055 mM PREDN, containing 0.050 mM Fe(III)-DTPA (1:2) at pH 7, 10 mA cm^{-2} and 25 °C.

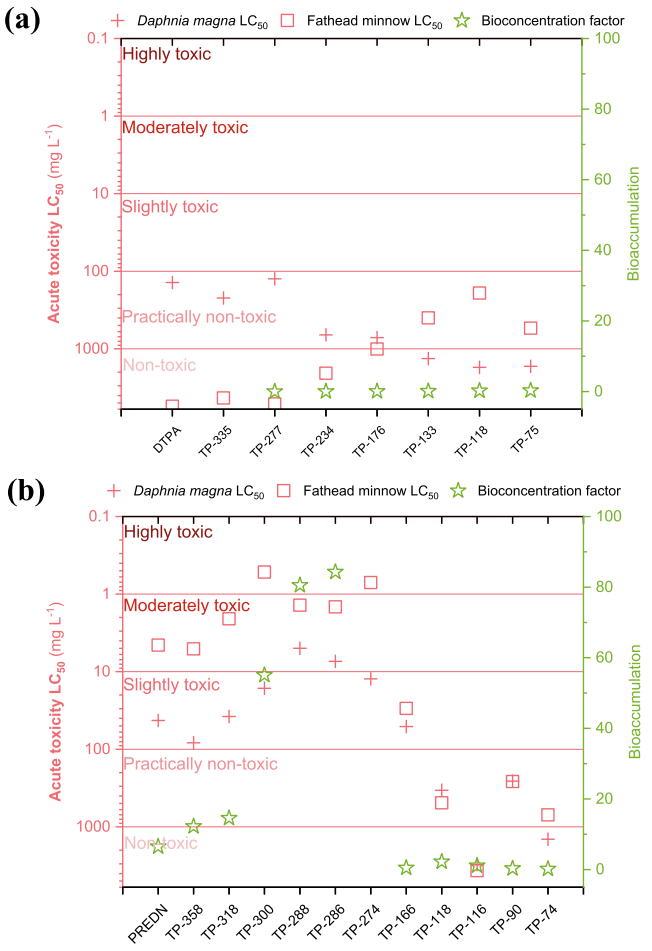

Fig. 8. Ecotoxicity and bioaccumulation profiles for: (a) DTPA and (b) PREDN and its associated TPs. The inverted left Y-axis (base-10 logarithmic scale) displays the acute toxicity LC_{50} (mg L^{-1}) for *Daphnia magna* and Fathead minnow. Dashed horizontal reference lines denote standardized U.S. EPA regulatory ecotoxicity thresholds [63]. The linear right Y-axis displays the absolute bioconcentration factor (BCF) to track the evolution of effluent bioaccumulation potential. *Note: Missing BCF for TP-274, DTPA and TP-335 indicates values outside the mathematical applicability domain of the QSAR model.*

Other studies also reported that DTPA and its by-products are non-toxic and, in fact, this chelating agent has been widely used as a fertilizer with ability to stimulate seed growth [26,31]. In the case of PREDN molecule and its derived photooxidation products, some studies have also demonstrated low toxicological risk in certain aquatic organisms such as *Daphnia magna*, *Thamnocephalus platyurus*, *Brachionus calyciflorus*, *Vibrio fischeri*, *Pseudokirchneriella subcapitata* [9,59]. Nonetheless, it is important to emphasize the necessity of removing this drug residue from water bodies due to its adverse effects on human health; PREDN could be unintentionally consumed through contaminated drinking water, fish meat, or aquatic plants.

Additionally, BOD_5 analyses revealed a slight increase between the initial and final sampling points (0 min and 90 min), rising from 17 to 21 mg O_2 L^{-1}, in the complete system. This moderate increase indicates

the formation of oxidation by-products that are more biodegradable than the parent compound. On the other hand, no change in BOD_5 was observed in the control system, yielding 19 mg O_2 L^{-1} for both the initial and final time, which reinforces the idea that the increase in biodegradability is solely associated with the degradation of PREDN and not due to any decomposition or transformation of the complex (Fig. S13). Crucially, the progressive generation of biodegradable oxalic acid (TP-90) could also serve as a stabilization mechanism [60–62]; it acts as a coordinating ligand forming iron-oxalate complexes, explaining how active dissolved iron is sustained in the bulk solution even after 95% of the primary Fe(III)-DTPA undergoes degradation via carboxymethyl dealkylation into non-toxic amino acid intermediates.

These combined results provide valuable insights into the environmental safety and performance of the SPEF process using DTPA as a chelating agent. The performance of the control system, both in terms of phytotoxicity and BOD_5, supports its stable behavior and non-toxic nature under the tested conditions. Meanwhile, the improvement in biodegradability and non-residual toxicity in the complete system suggests that the degradation of both PREDN and DTPA proceeds toward the formation of less harmful by-products over time. This approach, despite its intrinsic limitations related to isolating the full complexity of transformation pathways, offers a practical and effective framework to differentiate the individual contributions of the target contaminant and the iron complex. Thus, it enables a more accurate evaluation of the process, strongly supporting that it is not only efficient in degrading the contaminant but also stable and environmentally safe.

4. Conclusions

The stability of Fe(III)-DTPA complex and its catalytic efficiency in electron-driven water treatment were thoroughly evaluated, with SPEF as target process due to its inherently greener characteristics. The optimization of the Fe(III)-DTPA molar ratio demonstrated that, at 1:2, complete chelation of iron is accomplished at different pH values, which allows maintaining excellent stability under UVA and solar irradiation, as well as strong resistance to $^{\bullet}OH$-mediated oxidation. When this complex was used as homogeneous catalyst in SPEF process, the complex led to complete degradation of the glucocorticoid PREDN, with very low iron precipitation. The great ability of Fe(III)-DTPA (1:2) complex to maintain iron in solution, combined with its effectiveness to degrade glucocorticoids, sets it apart as a potential catalyst for advanced electrochemical wastewater treatment operating under near-neutral or variable pH conditions. Furthermore, the transformed products of both PREDN and DTPA were found to be biodegradable, and non-toxic to *Lactuca sativa*, despite a mid-stage pronounced relative toxicity, confirming the environmental safety of this approach. From this study, DTPA emerges as a promising and sustainable chelating agent to enhance the performance of EAOPs in actual wastewater treatment applications.

Declaration of competing interest

The authors declare the following financial interests/personal relationships which may be considered as potential competing interests: Ignasi Sires reports equipment, drugs, or supplies was provided by State Agency of Research. If there are other authors, they declare that they have no known competing financial interests or personal relationships that could have appeared to influence the work reported in this paper.

Acknowledgments

The authors are grateful to the following projects: PID2022-140378OB-I00, funded by MICIU/AEI/10.13039/501100011033 (Spain) and by ERDF/EU; project 2025ICREA00086, funded by the *Departament de Recerca i Universitats* (Generalitat de Catalunya, Spain) under Acadèmia d'Excel·lència Program; project 2023YFE0108100, supported by National Key Research and Development Program International Cooperation Project (China). P.T. acknowledges her FPI PhD scholarship (PRE2020-095114, MICINN, Spain), co-financed by ESF (EU). I.D.-R. acknowledges his PREDOCS-UB 2023 scholarship EFUP0JA021/UP0JA021, co-funded by the University of Barcelona and Banco Santander.

Appendix A. Supplementary data

Supplementary data to this article can be found online at https://doi.org/10.1016/j.seppur.2026.139404.

Data availability

Data will be made available on request.

References

[1] J.H. Jonkers, C.J. Houtman, Y. van Oorschot, M.H. Lamoree, T. Hamers, Identification of antimicrobial and glucocorticoid compounds in wastewater effluents with effect-directed analysis, Environ. Res. 231 (2023) 116117, https://doi.org/10.1016/j.envres.2023.116117.

[2] M.M.S. Yazdan, M.T. Ahad, Z. Mallick, S.P. Mallick, I. Jahan, M. Mazumder, An overview of the glucocorticoids' pathways in the environment and their removal using conventional wastewater treatment systems, Pollutants 1 (2021) 141–155, https://doi.org/10.3390/pollutants1030012.

[3] M. Mallek, D. Barceló, Advancing water treatment and reuse technologies to address the nexus of climate change, water scarcity, and pharmaceutical contamination, J. Environ. Chem. Eng. 13 (2025) 119284, https://doi.org/10.1016/j.jece.2025.119284.

[4] A.R. Cole, B.W. Brooks, Global occurrence of synthetic glucocorticoids and glucocorticoid receptor agonistic activity, and aquatic hazards in effluent discharges and freshwater systems, Environ. Pollut. 329 (2023) 121638, https://doi.org/10.1016/j.envpol.2023.121638.

[5] A. Zhang, X. Jiang, Q. Wang, S. Hao, D. Zhu, J. Wang, C. Wang, M. Liu, Assessment of glucocorticoid removal by UVA/chlorination and ozonation: performance comparison in kinetics, degradation pathway, and toxicity, Water 14 (2022) 2493, https://doi.org/10.3390/w14162493.

[6] N. Inarmal, B. Moodley, Selected pharmaceutical analysis in wastewater treatment plant during COVID-19 infection waves in South Africa, Environ. Sci.: Water Res. Technol. 9 (2023) 1566–1576, https://doi.org/10.1039/d3ew00059a.

[7] M.M.S. Yazdan, R. Kumar, S.W. Leung, The environmental and health impacts of steroids and hormones in wastewater effluent, as well as existing removal technologies : A review, Ecologies 3 (2022) 206–224, https://doi.org/10.3390/ecologies3020016.

[8] M.A. Lima e Silva, R. Lorca da Silva, T.P. Teixeira, T.L. Rocha, M. Marcon, Glucocorticoids as emerging pollutants in surface water: a systematic review on their global occurrence and distribution, Environ. Res. 273 (2025) 121280, https://doi.org/10.1016/j.envres.2025.121280.

[9] K. Yin, Q. He, C. Liu, Y. Deng, Y. Wei, S. Chen, T. Liu, S. Luo, Prednisolone degradation by UV/chlorine process: influence factors, transformation products and mechanism, Chemosphere 212 (2018) 56–66, https://doi.org/10.1016/J.chemosphere.2018.08.032.

[10] A.C. Miruka, A. Zhang, Q. Wang, D. Zhu, Z. Wang, Z. Sun, P. Héroux, Y. Liu, Degradation of glucocorticoids in water by a synergistic system of peroxymonosulfate, microbubble and dielectric barrier discharges, J. Water Process Eng. 42 (2021) 102175, https://doi.org/10.1016/j.jwpe.2021.102175.

[11] I.C. Tanui, F. Kandie, M. Krauss, A. Piotrowska, S. Finckh, A. Kiprop, H. Hollert, N. Shahid, M. Liess, W. Brack, Occurrence and potential risk of steroid hormones in selected surface water and wastewater treatment plants in western Kenya, Environ. Pollut. 367 (2025) 125623, https://doi.org/10.1016/j.envpol.2024.125623.

[12] H.N. Tien, F.M. Mwazighe, Preparation of Ti/SnO_2–Sb/La-βPbO_2 electrode and its application in the degradation of some pollutants including prednisolone and 8-hydroxyquinoline, Chemosphere 333 (2023) 138933, https://doi.org/10.1016/j.chemosphere.2023.138933.

[13] Q. Yuan, S. Qu, R. Li, Z.-Y. Huo, Y. Gao, Y. Luo, Degradation of antibiotics by electrochemical advanced oxidation processes (EAOPs): performance, mechanisms, and perspectives, Sci. Total Environ. 856 (2023) 159092, https://doi.org/10.1016/j.scitotenv.2022.159092.

[14] S. Mohammadi, M. Zarei, M.S. Amini-Fazl, M. Ebratkhahan, Removal and mineralization of prednisolone from water by using homogeneous and heterogeneous electro-Fenton process, J. Environ. Chem. Eng. 11 (2023) 110465, https://doi.org/10.1016/j.jece.2023.110465.

[15] P. Xia, H. Zhang, Z. Ye, Recent advances in the application of natural iron and clay minerals in heterogeneous electro-Fenton process, Curr. Opin. Electrochem. 46 (2024) 101495, https://doi.org/10.1016/j.coelec.2024.101495.

[16] C.A. Martínez-Huitle, M.A. Rodrigo, I. Sirés, O. Scialdone, A critical review on latest innovations and future challenges of electrochemical technology for the abatement of organics in water, Appl. Catal. B: Environ. 328 (2023) 122430, https://doi.org/10.1016/j.apcatb.2023.122430.

[17] P. La Manna, M. De Carluccio, P. Iannece, G. Vigliotta, A. Proto, L. Rizzo, Chelating agents supported solar photo-Fenton and sunlight/H_2O_2 processes for pharmaceuticals removal and resistant pathogens inactivation in quaternary treatment for urban wastewater reuse, J. Hazard. Mater. 452 (2023) 131235, https://doi.org/10.1016/j.jhazmat.2023.131235.
[18] F. Deng, H. Olvera-Vargas, M. Zhou, S. Qiu, I. Sirés, E. Brillas, Critical review on the mechanisms of Fe^{2+} regeneration in the electro-Fenton process: fundamentals and boosting strategies, Chem. Rev. 123 (2023) 4635–4662, https://doi.org/10.1021/acs.chemrev.2c00684.
[19] J.C. Murillo-Sierra, E. Ruiz-Ruiz, L. Hinojosa-Reyes, J.L. Guzmán-Mar, F. Machuca-Martínez, A. Hernández-Ramírez, Sulfamethoxazole mineralization by solar photo electro-Fenton process in a pilot plant, Catal. Today 313 (2018) 175–181, https://doi.org/10.1016/j.cattod.2017.11.003.
[20] G. Coria, T. Pérez, I. Sirés, E. Brillas, J.L. Nava, Abatement of the antibiotic levofloxacin in a solar photoelectro-Fenton flow plant: modeling the dissolved organic carbon concentration-time relationship, Chemosphere 198 (2018) 126198, doi:https://doi.org/10.1016/j.chemosphere.2018.01.112.
[21] E. Brillas, Solar photoelectro-Fenton : A very effective and cost-efficient electrochemical advanced oxidation process for the removal of organic pollutants from synthetic and real wastewaters, Chemosphere 327 (2023) 138532, https://doi.org/10.1016/j.chemosphere.2023.138532.
[22] N. Klamerth, S. Malato, A. Agüera, A. Fernández-Alba, Photo-Fenton and modified photo-Fenton at neutral pH for the treatment of emerging contaminants in wastewater treatment plant effluents: A comparison, Water Res. 47 (2013) 833–840, https://doi.org/10.1016/j.watres.2012.11.008.
[23] A. De Luca, R.F. Dantas, S. Esplugas, Assessment of iron chelates efficiency for photo-Fenton at neutral pH, Water Res. 61 (2014) 232–242, https://doi.org/10.1016/j.watres.2014.05.033.
[24] E. Cuervo Lumbaque, D. Salmoria Araújo, T. Moreira Klein, E.R. Lopes Tiburtius, J. Argüello, C. Sirtori, Solar photo-Fenton-like process at neutral pH: Fe(III)-EDDS complex formation and optimization of experimental conditions for degradation of pharmaceuticals, Catal. Today 328 (2019) 259–266, https://doi.org/10.1016/j.cattod.2019.01.006.
[25] U.J. Ahile, R.A. Wuana, A.U. Itodo, R. Sha'Ato, R.F. Dantas, A review on the use of chelating agents as an alternative to promote photo-Fenton at neutral pH: current trends, knowledge gap and future studies, Sci. Total Environ. 710 (2020) 134872, https://doi.org/10.1016/j.scitotenv.2019.134872.
[26] N. López-Vinent, A. Cruz-Alcalde, J. Giménez, S. Esplugas, Mixtures of chelating agents to enhance photo-Fenton process at natural pH : influence of wastewater matrix on micropollutant removal and bacterial inactivation, Sci. Total Environ. 786 (2021) 147416, https://doi.org/10.1016/j.scitotenv.2021.147416.
[27] I. Salmerón, P. Núñez-Tafalla, S. Venditti, J. Hansen, Operational challenges in scaling photo-Fenton at neutral pH: toward real-scale urban wastewater purification, J. Environ. Chem. Eng. 14 (2026) 120574, https://doi.org/10.1016/j.jece.2025.120574.
[28] A. De Luca, R.F. Dantas, S. Esplugas, Study of Fe(III)-NTA chelates stability for applicability in photo-Fenton at neutral pH, Appl. Catal. B: Environ. 179 (2015) 372–379, https://doi.org/10.1016/j.apcatb.2015.05.025.
[29] U.J. Ahile, R.A. Wuana, A.U. Itodo, R. Sha'Ato, R.F. Dantas, Stability of iron chelates during photo-Fenton process: the role of pH, hydroxyl radical attack and temperature, J. Water Process Eng. 36 (2020) 101320, https://doi.org/10.1016/j.jwpe.2020.101320.
[30] U.J. Ahile, R.A. Wuana, A.U. Itodo, R. Sha'Ato, J.A. Malvestiti, R.F. Dantas, Stability and efficiency of Fe^{3+} EDDS complex for the treatment of secondary effluent in the photo-Fenton process, Desalin. Water Treat. 222 (2021) 366–374, https://doi.org/10.5004/dwt.2021.27081.
[31] N. López-Vinent, A. Cruz-Alcalde, J.A. Malvestiti, P. Marco, J. Giménez, S. Esplugas, Organic fertilizer as a chelating agent in photo-Fenton at neutral pH with LEDs for agricultural wastewater reuse: micropollutant abatement and bacterial inactivation, Chem. Eng. J. 388 (2020) 124246, https://doi.org/10.1016/J.CEJ.2020.124246.
[32] N. López-Vinent, A. Cruz-Alcalde, J. Giménez, S. Esplugas, C. Sans, Improvement of the photo-Fenton process at natural condition of pH using organic fertilizers mixtures: potential application to agricultural reuse of wastewater, Appl. Catal. B: Environ. 290 (2021) 120066, https://doi.org/10.1016/j.apcatb.2021.120066.
[33] P. Prete, A. Fiorentino, L. Rizzo, A. Proto, R. Cucciniello, Review of aminopolycarboxylic acids–based metal complexes application to water and wastewater treatment by (photo-)Fenton process at neutral pH, Curr. Opinion Green Sustain. Chem. 28 (2021) 100451, https://doi.org/10.1016/j.cogsc.2021.100451.
[34] E. Cuervo Lumbaque, R.M. Cardoso, A. de Araújo Gomes, S. Malato, J.A. Sánchez Pérez, C. Sirtori, Removal of pharmaceuticals in hospital wastewater by solar photo-Fenton with Fe^{3+}-EDDS using a pilot raceway pond reactor: transformation products and *in silico* toxicity assessment, Microchem. J. 164 (2021) 106014, https://doi.org/10.1016/j.microc.2021.106014.
[35] E.M. Jiménez-Bambague, C.A. Madera-Parra, M.F. Rangel-Delgado, I. Quintero-Martínez, D. Miranda-Mosquera, J.S. Aristizabal-Apolinar, F. Machuca-Martínez, Photo-Fenton and electro-Fenton performance for the removal of pharmaceutical compounds in real urban wastewater, Electrochim. Acta 442 (2023) 141905, https://doi.org/10.1016/j.electacta.2023.141905.
[36] Z. Ye, E. Brillas, F. Centellas, P.L. Cabot, I. Sirés, Electro-Fenton process at mild pH using Fe(III)-EDDS as soluble catalyst and carbon felt as cathode, Appl. Catal. B: Environ. 257 (2019) 117907, https://doi.org/10.1016/j.apcatb.2019.117907.
[37] Z. Ye, E. Brillas, F. Centellas, P.L. Cabot, I. Sirés, Expanding the application of photoelectro-Fenton treatment to urban wastewater using the Fe(III)-EDDS complex, Water Res. 169 (2020) 115219, https://doi.org/10.1016/j.watres.2019.115219I.C.
[38] I. Da Costa Soares, R. Oriol, Z. Ye, C.A. Martínez-Huitle, P.L. Cabot, E. Brillas, I. Sirés, Photoelectro-Fenton treatment of pesticide triclopyr at neutral pH using Fe (III)–EDDS under UVA light or sunlight, Environ. Sci. Pollut. Res. 28 (2021) 23833–23848, https://doi.org/10.1007/s11356-020-11421-8.
[39] N. López-Vinent, A. Cruz-Alcalde, C. Lai, J. Giménez, S. Esplugas, C. Sans, Role of sunlight and oxygen on the performance of photo-Fenton process at near neutral pH using organic fertilizers as iron chelates, Sci. Total Environ. 803 (2022) 149873, https://doi.org/10.1016/j.scitotenv.2021.149873.
[40] J. Xiao, Y. Li, H. Dong, Z. Pang, M. Zhao, J. Dong, D. Huang, L. Li, Diethylenetriaminepentaacetic acid (DTPA)-reinforced Fenton-like process for efficient abatement of sulfamethazine at circumneutral pH in simulated groundwater, Sep. Purif. Technol. 336 (2024) 126266, https://doi.org/10.1016/j.seppur.2024.126266.
[41] I.S.S. Pinto, I.F.F. Neto, H.M.V.M. Soares, Biodegradable chelating agents for industrial, domestic, and agricultural applications—a review, Environ. Sci. Pollut. Res. 21 (2014) 11893–11906, https://doi.org/10.1007/s11356-014-2592-6.
[42] M. Yorlady, A. Zuluaga, M. Cardarelli, Y. Rouphael, S. Cesco, Y. Pii, G. Colla, Iron nutrition in agriculture: from synthetic chelates to biochelates, Sci. Hortic. 312 (2023) 111833, https://doi.org/10.1016/j.scienta.2023.111833.
[43] S. Chen, L. An, S. Yang, Low-molecular-weight Fe(III) complexes for MRI contrast agents, Molecules 27 (2022) 4573, https://doi.org/10.3390/molecules27144573.
[44] F. Zucconi, A. Pera, M. Forte, M. De Bertoldi, Evaluating toxicity of immature compost, Biocycle 22 (1981) 54–57.
[45] F. Zucconi, M. Forte, A. Monaco, M. De Bertoldi, Biological evaluation of compost maturity, Biocycle 22 (1981) 27–29.
[46] US. EPA, Protocols for short term toxicity screening of hazardous waste sites. A. 8.7, Lettuce root elongation (Latuca sativa), EUA, Chicago, 1989.
[47] N.F.Y. Tam, S. Tiquia, Assessing toxicity of spent pig litter using a seed germination technique, Resour. Conserv. Recycl. 11 (1994) 261–274, https://doi.org/10.1016/0921-3449(94)90094-9.
[48] APHA, AWWA, WEF, 5210-D: Respirometric method: Biochemical oxygen demand (BOD), in: Standard methods for the examination of water and wastewater, am. Public Heal. Assoc., Washington, D.C., 2023.
[49] A. Liu, Y. Liu, C. Luo, C. Wang, L. Dong, Z. Zhu, J. Qiang, Study on the synergistic removal of metal ions by study on the synergistic removal of metal ions by 18-crown-6 and diethylenetriaminepentaacetic acid in barrier layer chemical mechanical polishing, ECS J. Solid State Sci. Technol. 14 (2025) 124004, https://doi.org/10.1149/2162-8777/ae2d97.
[50] A. De Luca, Fenton and Photo-Fenton like at Neutral pH for the Removal of Emerging Contaminants in Water and Wastewater Effluents, Universitat de Barcelona, 2016.
[51] S. Jaber, M. Leremboure, V. Thery, A.-M. Delort, G. Mailhot, Mechanism of photochemical degradation of Fe(III)-EDDS complex, J. Photochem. Photobiol. A Chem. 399 (2020) 112646, https://doi.org/10.1016/j.jphotochem.2020.112646.
[52] S. Krishnan, C.A. Martínez-Huitle, P.V. Nidheesh, An overview of chelate modified electro-Fenton processes, J. Environ. Chem. Eng. 10 (2022) 107183, https://doi.org/10.1016/j.jece.2022.107183.
[53] H.H.-H. Lin, A.Y.-C. Lin, Solar photo-Fenton oxidation of cytostatic drugs via Fe (III)-EDDS at circumneutral pH in an aqueous environment, J. Water Process Eng. 41 (2021) 102066, https://doi.org/10.1016/j.jwpe.2021.102066.
[54] G.V. Buxton, C.L. Greenstock, W.P. Helman, A.B. Ross, Critical review of rate constants for wreactions of hydrated electrons, hydrogen atoms and hydroxyl radicals (˙OH/˙O⁻) in aqueous solution, J. Phys. Chem. Ref. Data Monogr. 17 (1988) 513–886, https://doi.org/10.1063/1.555805.
[55] S. Arzate, M.C. Campos-Mañas, S. Miralles-Cuevas, A. Agüera, J.L. García Sánchez, J.A. Sánchez Pérez, Removal of contaminants of emerging concern by continuous flow solar photo-Fenton process at neutral pH in open reactors, J. Environ. Manag. 261 (2020) 110265, https://doi.org/10.1016/j.jenvman.2020.110265.
[56] A.M. Díez, A.S. Ribeiro, M.A. Sanromán, M. Pazos, Optimization of photo-Fenton process for the treatment of prednisolone, Environ. Sci. Pollut. Res. 25 (2018) 27768–27782, https://doi.org/10.1007/s11356-018-1782-z.
[57] B. Almazrouei, D. Islayem, F. Alskafi, M.K. Catacutan, R. Amna, S. Nasrat, B. Sizirici, I. Yildiz, Steroid hormones in wastewater: sources, treatments, environmental risks, and regulations, Emerg. Contam. 9 (2023) 100210, https://doi.org/10.1016/j.emcon.2023.100210.
[58] K.A. Hossain, K. Roy, Chemometric modeling of aquatic toxicity of contaminants of emerging concern (CECs) in Dugesia japonica and its interspecies correlation with daphnia and fish: QSTR and QSTTR approaches, Ecotox. Environ. Safety 166 (2018) 92–101, https://doi.org/10.1016/j.ecoenv.2018.09.068.
[59] M. DellaGreca, A. Fiorentino, M. Isidori, M. Lavorgna, L. Previtera, M. Rubino, F. Temussi, Toxicity of prednisolone, dexamethasone and their photochemical derivatives on aquatic organisms, Chemosphere 54 (2004) 629–637, https://doi.org/10.1016/j.chemosphere.2003.09.008.
[60] R. Paris, K. V. Desboeufs, Effect of atmospheric organic complexation on iron-bearing dust solubility, Atmos. Chem. Phys. 13(9) 82013) 4895–4905, doi: https://doi.org/10.5194/acp-13-4895-2013.
[61] G. Zhang, Q. Lin, L. Peng, Y. Yang, F. Jiang, F. Liu, W. Song, D. Chen, Z. Cai, X. Bi, M. Miller, M. Tang, W. Huang, X. Wang, P. Peng, G. Sheng, Oxalate formation

enhanced by Fe-containing particles and environmental implications, Environ. Sci. Technol. 53 (3) (2019) 1269–1277, https://doi.org/10.1021/acs.est.8b05280 24.
[62] Y.G. Zuo, J. Hoigne, Formation of hydrogen-peroxide and depletion of oxalic-acid in atmospheric water by photolysis of iron(iii) oxalato complexes, Environ. Sci. Technol. 26 (5) (1992) 1014–1022, https://doi.org/10.1021/es00029a022.
[63] Appendix I. Toxicity Categories and LOCs by the United States Environmental Protection Agency (U.S. EPA) - epa.gov/pesticides/endanger/litstatus/effects/redleg-frog/naled/appendix-i.pdf [Consulted on: 23/06/2026].